

Heavy ion irradiation effects on GaN/AlGaN high electron mobility transistor failure at off-state

Zahabul Islam^a, Angela L. Paoletta^b, Anthony M. Monterrosa^c, Jennifer D. Schuler^d, Timothy J. Rupert^d, Khalid Hattar^c, Nicholas Glavin^e, Aman Haque^{a,*}

^a Department of Mechanical Engineering, The Pennsylvania State University, University Park, PA 16802, USA

^b Department of Chemistry, Princeton University, Princeton, NJ 08540, USA

^c Sandia National Laboratories, PO Box 5800-1056, Albuquerque, NM 87185, USA

^d Department of Materials Science and Engineering, University of California, Irvine, CA 92697, USA

^e Air Force Research Laboratory, Materials and Manufacturing Directorate, 2941 Hobson Way, Wright-Patterson AFB, OH 45433, USA



ARTICLE INFO

Keywords:

Ion irradiation

High electron mobility transistor (HEMT)

In-situ transmission electron microscopy (in-situ TEM)

Energy dispersive X-ray spectroscopy (EDS)

ABSTRACT

We investigate the effects of ion irradiation on AlGaN/GaN high electron mobility transistors using in-situ transmission electron microscopy. The experiments are performed inside the microscope to visualize the defects, microstructure and interfaces of ion irradiated transistors during operation and failure. Experimental results indicate that heavy ions such as Au⁴⁺ can create a significant number of defects such as vacancies, interstitials and dislocations in the device layer. It is hypothesized that these defects act as charge traps in the device layer and the resulting charge accumulation lowers the breakdown voltage. Sequential energy dispersive X-ray spectroscopy mapping allows us to track individual chemical elements during the experiment, and the results suggest that the electrical degradation in the device layer may originate from oxygen and nitrogen vacancies.

1. Introduction

GaN based high-electron mobility transistors (HEMT) are strong candidates for next generation electronics such as power amplifiers, broadband communication and high-voltage switches due to their high breakdown voltage and wide-bandgap [1,2]. The unique feature of the HEMTs is the channel that is essentially a two dimensional electron gas (2DEG) [3]. The high carrier density and mobility of the channel yield low on-resistance which reduces switching losses when operated in switching mode power converter [4]. In addition, the wide bandgap of GaN allows operation at high electrical and temperature fields [5]. Such robustness of GaN HEMT makes them an attractive choice for harsh environment applications [6,7].

Due to their size, weight and power effectiveness, GaN HEMTs are attractive for space applications. High energy particles feature the cosmic rays or solar flares in space, with energies up to 100 MeV for the protons, and up to 10 GeV for heavy ions [8]. They create electron-hole pairs and displace atoms from their original lattice position, leaving vacancies, interstitials and dislocations in the crystal [9]. Over time, these defects accumulate and interact with each other to generate stacking faults, dislocation loops, and vacancy/interstitial clusters

[10,11]. Such microstructural degradation influence performance through increased threshold voltage, leakage current and decreased mobility [12]. Other suggested changes are lower carrier density and mobility in the 2DEG sheet [3] and decrease of the Schottky barrier height at the gate [13].

The need for radiation tolerant electronics for space applications has motivated fundamental studies on wide bandgap materials that are superior compared to Si devices because of the higher displacement and bond energies [14]. Ionization effects in GaN are not as severe due to the absence of gate dielectric in the HEMT structure and the higher surface state density in GaN [15]. Khanna et al. [6] studied 2 MeV proton radiation damage in GaN films using low temperature photoluminescence spectroscopy at different fluences ranging from 10⁹ to 10¹⁵ proton/cm². Their measurement shows that the fluence required for equal amount of excitonic intensity reduction in GaAs is 10¹³ proton/cm², whereas for GaN it is 10¹⁵ proton/cm². These low temperature photoluminescence intensity measurements indicate the evidence of high radiation tolerance of GaN compared to GaAs. Metallic-to-insulator transition in 2DEG in AlGaAs/GaAs is studied by Gaudreau et al. [7]. Their 2 MeV proton study shows that fluence required for metallic-to-insulator transition in AlGaAs/GaAs is two orders of

* Corresponding author.

E-mail address: mah37@psu.edu (A. Haque).

magnitude lower compared to AlGaN/GaN for similar level of transition. This measurement of transport properties of proton-irradiated GaN-based 2DEG also supports the radiation tolerant properties of GaN compared to GaAs.

In addition to films, significant amount of work has been done on radiation damage in GaN-based devices. Karmarkar et al. [16] studied 1.8 MeV proton induced radiation damage in AlGaN/GaN HEMT up to 10^{15} proton/cm² fluence. They measured device performance in terms of sheet carrier mobility, sheet carrier density, resistance of the thin film structure, and Schottky barrier height at the gate, and their observations show that devices exhibit good tolerance up to 10^{14} proton/cm² fluence. White et al. [17] characterized AlGaN/GaN HEMT at 1.8 MeV proton irradiation to show that carrier mobility and carrier density are radiation tolerant up to 10^{14} and 10^{15} proton/cm² fluence respectively. However, the exact mechanism(s) for degradation and their signatures in the transistor characteristics remain to be resolved in the literature. This is manifested through the variation in the dose dependence of device operation and failure. For example, the literature contains evidence of a decrease in DC saturation current and transconductance at a fluence of 10^{14} cm⁻² protons or even at lower dose such as 10^{12} cm⁻² [15,18]. Cai et al. [18] studied the effect of 1.8 MeV proton irradiation on the properties of an AlGaN/GaN HEMT using current-voltage (I-V) characteristics and Raman scattering measurements. Their study indicates 62% and 68% decrease in saturation current and transconductance respectively at 1.8 MeV proton irradiation with 10^{14} proton/cm² fluence. Hu et al. [15] investigated the effects of proton irradiation at various energies for AlGaN/GaN HEMTs, and they observed 10.6% and 6.1% decrease in drain saturation current and transconductance respectively at 1.8 MeV irradiation of proton with a fluence of 10^{12} proton/cm². These studies indicate that irradiation effects on GaN HEMTs can be significant.

The current trend in the literature is to measure these electrical parameters ex-situ as a function of radiation dose and then analyze the data to identify signatures of failure mechanisms based on device models [19]. Pinpointing the dominant mechanism is the most difficult part of the analysis where in-situ microscopy can be of tremendous help. This is reflected by studies performing dissection of the HEMT specimens after the experiment is over and then using microscopy techniques to investigate regions of interest to recreate the evolution of failure mechanisms. Such post-experiment or post-mortem (after the HEMT has failed) microscopy is useful in validating any hypothesis on the effects of radiation induced defects. Post-mortem microscopy can indicate the extent of radiation damage, but it cannot capture their interaction with the defects generated due to the very high electrical, mechanical and thermal fields during HEMT operation. As a HEMT swings between on (high electrical and thermal field) and off (high electrical field) states, defects and traps are generated even without radiation. This is expected to be exacerbated with the presence of radiation induced defects. We suggest that in-situ microscopy could be helpful in resolving this concern. Here, the HEMT is electrically characterized inside a microscope that allows in-situ irradiation as well as microstructural observation in real time.

In this study, we demonstrate in-situ transmission electron microscopy (TEM) for simultaneous quantitative and qualitative characterization of GaN HEMTs. We characterized both pristine and Au⁴⁺ irradiated GaN HEMTs die and electron transparent coupons using a semiconductor parametric analyzer and TEM respectively. The achievable damage rates in terms of displacement per atom or dpa ($\sim 10^{-3}$ dpa/s) are higher in ion irradiation compared to the typical $\sim 10^{-7}$ dpa/s for nuclear reactors, which saves experimental time and cost [20]. Atomic resolution imaging accompanied by energy dispersive x-ray spectroscopy (EDS) and electron diffraction make simultaneous quantitative characterization and qualitative visualization possible. Thus, our in-situ study not only provides invaluable information on heavy ion induced defects generation in GaN HEMTs, but it also predicts the performance and degradation mechanism of the device under

heavy ion irradiation in a harsh environment.

2. Experimental methods

To study the effect of ion irradiation on the electrical performance and failure of GaN HEMTs, we designed a series of experiments as described below.

- (a) Commercially acquired depletion mode GaN on SiC HEMTs (Wolfspeed, CGHV1J006D rated at 6 W, 18GHz and 40 V) were electrically characterized at die level. The DC mode transfer and output characteristics were obtained before irradiation using a Keithley 2400 semiconductor parametric analyzer at room temperature.
- (b) The pristine HEMT dies were irradiated ex-situ normal to the surface with 1.5 MeV Au⁺ ions using the 6 MV HVE Tandem accelerator at Sandia National Laboratories. The irradiated dies are then electrically characterized to compare the die-level performance degradation.
- (c) Electron transparent (~100 nm thick) HEMT specimens were prepared from the pristine dies using the focused ion beam (FIB) as described in [21,22]. These specimens were then in-situ ion-irradiated inside a TEM [23] to obtain a visual description of radiation induced defect generation.
- (d) Electron transparent HEMT specimens were prepared from the ex-situ ion irradiated dies and characterized for DC transfer and output characteristics inside a TEM. The specimens are electrically biased till failure while acquiring TEM images. Chemical elemental mapping was performed on the electron transparent HEMT before and after failure using energy dispersive X-ray spectroscopy (EDS) in the TEM.

The ex-situ ion irradiation was performed on three dies with fluences approximately 6.5×10^{13} , 6.5×10^{14} , and 6.5×10^{15} ions/cm². The ion energy was chosen based on a Stopping and Range of Ions in Matter (SRIM) simulation [24] to have a relatively uniform damage profile in the device layers. Irradiation damage level in term of dpa were 0.45, 4.5, and 45.0 dpa for each respective fluence level.

During the preparation of the electron transparent specimens, special care was taken during the final thinning phase to minimize the FIB damage and to keep the three electrodes (i.e drain, gate and source) intact. In addition, the transfer process of thin specimen from a custom TEM grid to a micro-electro-mechanical (MEMS) device requires low accelerating voltage and ion beam current exposure to avoid any damage in the device layer. Fig. 1b shows a mounted chip on a TEM specimen holder with electrical biasing capability. Details of the MEMS chip design and capability are described elsewhere [25]. Fig. 1c shows the electron transparent thin sample on the TEM grid prior to the integration with the MEMS chip. We performed in-situ TEM experiments in a 200 kV FEI Talos F200X S/TEM with 1.2 Å resolution.

High resolution transmission electron microscopy (HRTEM) was used to estimate the atomic-scale strain in the sample using geometric phase analysis technique (GPA) [26]. In the GPA technique, phase image, P_g can be expressed by the component of the displacement field, $u(\mathbf{r})$, in the direction of the reciprocal lattice vector \mathbf{g} :

$$P_g(\mathbf{r}) = -2\pi g u(\mathbf{r}) \quad (1)$$

A two-dimensional displacement field can be obtained from Eq. (1) by choosing two independent phase images (P_{g1} and P_{g2}):

$$\mathbf{u}(\mathbf{r}) = -\frac{1}{2\pi} [P_{g1}(\mathbf{r}) \mathbf{a}_1 + P_{g2}(\mathbf{r}) \mathbf{a}_2] \quad (2)$$

$$\begin{pmatrix} u_x \\ u_y \end{pmatrix} = -\frac{1}{2\pi} \begin{pmatrix} g_{1x} & g_{1y} \\ g_{2x} & g_{2y} \end{pmatrix}^{-1} \begin{pmatrix} P_{g1} \\ P_{g2} \end{pmatrix} \quad (3)$$

where P_{g1} and P_{g2} are two phase images, \mathbf{a}_1 and \mathbf{a}_2 are lattice vectors in

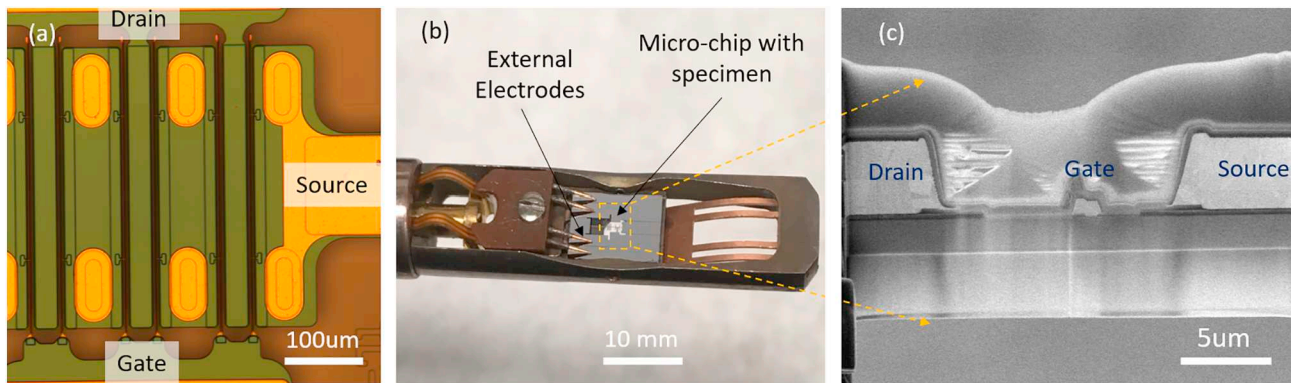


Fig. 1. Experimental setup for in-situ TEM operation of electron transparent HEMTs: (a) GaN HEMT die, (b) a MEMS chip with the HEMT specimen mounted on in-situ TEM electrical biasing holder, (c) FIB lamella of the HEMT before mounting on to the MEMS chip.

real space, u_x and u_y are displacement fields, g_x and g_y are two components of \mathbf{g} in reciprocal space. Once the displacement field is known, atomic strain map could be obtained from elasticity theory using the following equations:

$$\varepsilon_{xx} = \frac{\partial u_x}{\partial x} \quad (4a)$$

$$\varepsilon_{xy} = \frac{1}{2} \left(\frac{\partial u_x}{\partial y} + \frac{\partial u_y}{\partial x} \right) \quad (4b)$$

$$\varepsilon_{yy} = \frac{\partial u_y}{\partial y} \quad (4c)$$

where ε_{xx} , ε_{xy} and ε_{yy} are normal strain in x direction, shear strain in x-y plane and normal strain in y direction respectively.

3. Results and discussions

3.1. Die-level irradiation effects

Fig. 2a shows the irradiation direction in GaN HEMT die. Fig. 2b shows the SRIM simulation results on the damage level in dpa units as a function of depth into the device. The effect of ion irradiation is evident in Fig. 2c and d, which show bright field TEM images of a pristine HEMT and one irradiated at 45 dpa respectively. We compared high resolution images of irradiated specimens as shown in Fig. 2d with pristine counterparts to estimate the relative difference in dislocation density. Significantly higher (more than $100\times$) dislocation density was observed in the irradiated HEMTs, which is associated with the degraded performance measured by the parametric analyzer.

We then measured the performance of the pristine and irradiated HEMT in their bulk form. Fig. 3a shows their transfer characteristic curves. We notice that the threshold voltage (V_{th}) for a pristine HEMT is approximately -3.1 V. However, in case of all the irradiated HEMTs we do not see any significant increase in output current compared to the pristine counterpart during the gate voltage increment. This indicates that ion damage could not activate the gate, probably because of the damage in the 2DEG channel. To perform experiments in the off-state mode, we keep the gate voltage (V_g) at -5 V. Output characteristics curve of all the dies in the off-state are shown in Fig. 3b. Here, the output current is seen to reduce by about four orders of magnitude for the highest damage level (45 dpa). This drastic reduction in output current is attributed to the defect introduction in the AlGaN layer as well as the GaN layer during the Au^{4+} ion irradiation, which lead to lower carrier density and mobility in the 2DEG channel. We also notice that the output drain current significantly decreases with increasing irradiation dose.

3.2. In-situ ion irradiation effects (No biasing)

The objective of this set of experiments was primarily to visualize the irradiation induced defects in the lattice and interfaces of the HEMT system. These defects influence the device performance, since very large amount of thermal, electrical and mechanical stresses are generated during the HEMT operation. Fig. 4 shows snapshots of a specimen before and after exposure to 2.8 MeV Au^{4+} ion species for 60 min to a fluence of 4×10^{14} ions/ cm^2 . This is also shown in a supplementary video file (SV1), which shows shifts in sample contrast, particularly at the locations of pre-existing dislocations. The effect of ion bombardment is remarkable right under the gate, where the mechanical stress is also the highest. During an irradiation process interstitial atoms routinely leave their regular lattice sites and occupy interstitial sites. These interstitial atoms might appear as dark contrast in a BF TEM image [34]. Thus, the contrast change (dashed rectangular box in Fig. 4b) is an outcome of increased number of point defects. The effect of irradiation is also remarkable at the GaN-SiC interface. Fig. 4b shows how the initially sharp interface is deteriorated due to the appearance of dislocations (indicated by arrows) associated with it. It was not determined if these dislocations were a direct result of the radiation damage or resulted as a strain relief mechanism due to interface stress from the radiation damage.

3.3. In-situ TEM electrical characterization

In this series of experiments, we characterized the transfer and output functions of the electron transparent specimens inside the TEM. The specimens were prepared from the ex-situ irradiated dies because of the well-characterized nature of the irradiation simulation and boundary conditions. The objective is to visualize the defect and damage evolution processes under electrical biasing. Such in-situ analytical microscopy is attractive compared to post-mortem analysis since quantitative (device characterization) as well as qualitative (microscopic visualization) information can be acquired simultaneously. However, it is important to note that the electron transparent specimens have different aspect ratio and boundary conditions compared to the die-level specimens [27]. Hence, their transfer and output characteristics functions follow similar trend, which suggests that our in-situ TEM experiments can still be useful for capturing the mechanics and physics of degradation.

Fig. 5a shows drain current response of an irradiated sample during failure test. This data is shown for the transistor irradiated with highest damage (45 dpa). We observe that drain current recovers after each loading step up to a drain bias of 8 V. However, after an 8 V drain bias, the current shows large swings of fluctuation before failure at 10.2 V bias. Fig. 5a also labels 5 distinct data points (a, c, d, e, f), for which the

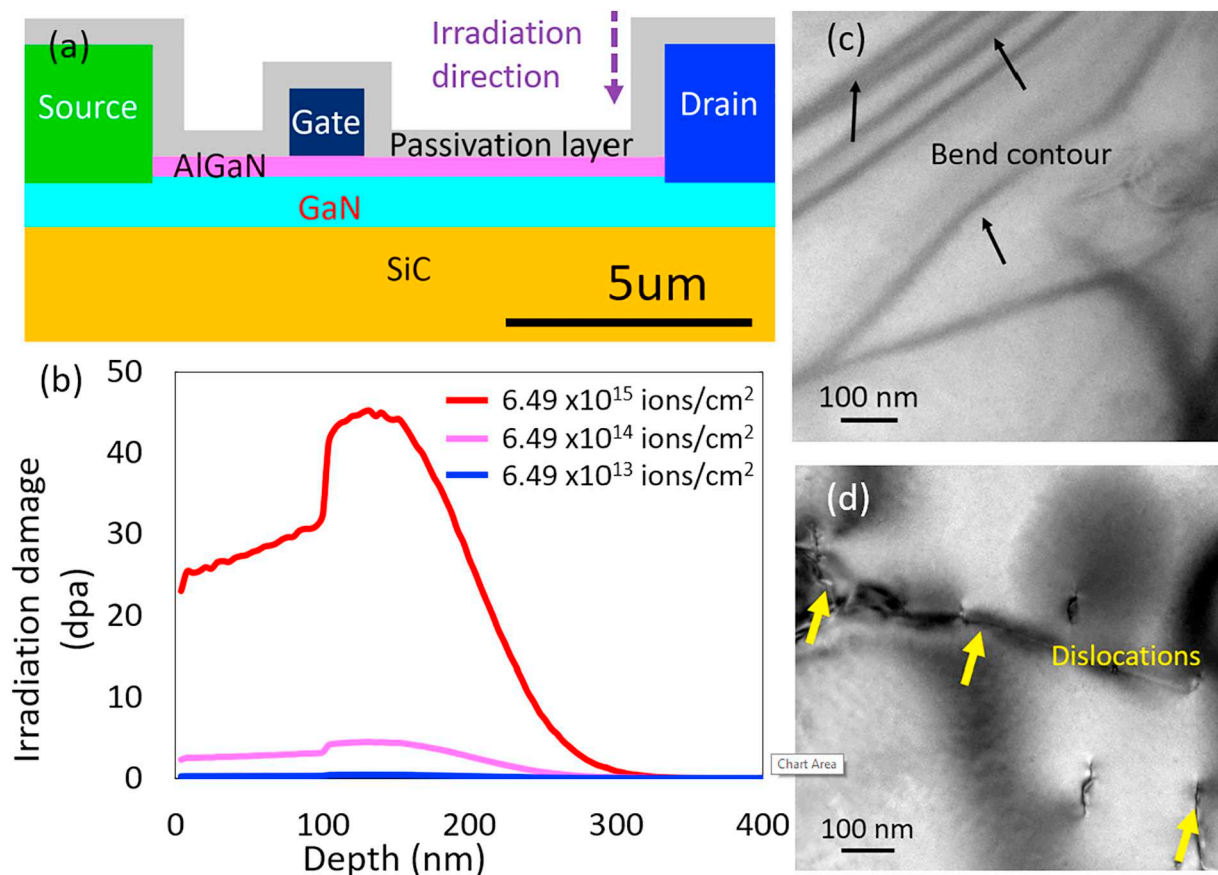


Fig. 2. (a) Schematic diagram of the GaN HEMT showing irradiation direction, (b) Displacement per atom (dpa) profile for different doses of irradiation, (c) TEM image of a pristine HEMT showing mostly bend contours (d) TEM image of an irradiated HEMT at 45 dpa showing very high dislocation density.

corresponding bright-field TEM images are presented in Fig. 6. A comparison between a pristine and an irradiated HEMT sample is shown in Fig. 5b. The pristine HEMT can operate with more than two times higher drain voltage compared to the irradiated sample, and drain current of the pristine HEMT is one order of magnitude higher than the irradiated HEMT. Drops in drain voltage and current could be attributed to the defects formation during an irradiation process [18,19].

Fig. 6 shows TEM images at different drain voltage bias during the off-state failure tests inside the TEM. These low magnification images show many bend contours as well as a number of defect clusters. Examples of these irradiation induced defects from the heavy ion Au⁴⁺ irradiation are shown at very high magnification in Fig. 6b. Atomic

resolution imaging enable us to observe this individual dislocations indicated by red colored perpendicular sign (⊥). The abundance of radiation induced defects was not seen in the pristine dies. Fig. 6c shows the HEMT at drain voltage of 5 V, which is large enough to trigger very minute changes in the drain current (note the location of point c in Fig. 5a). Events like these indicate highly localized microstructural damage that nucleate from preexisting defects, such as dislocations. For irradiated specimens, radiation damage can proliferate such nucleation. For pristine HEMTs, this damage usually takes place at the drain edge of the gate where the stress field is the maximum. The predominant features in Fig. 6 are the bend contours that arise from elastic bending during specimen preparation (due to the mechanical constrains at the drain, gate and source boundary). However, defects

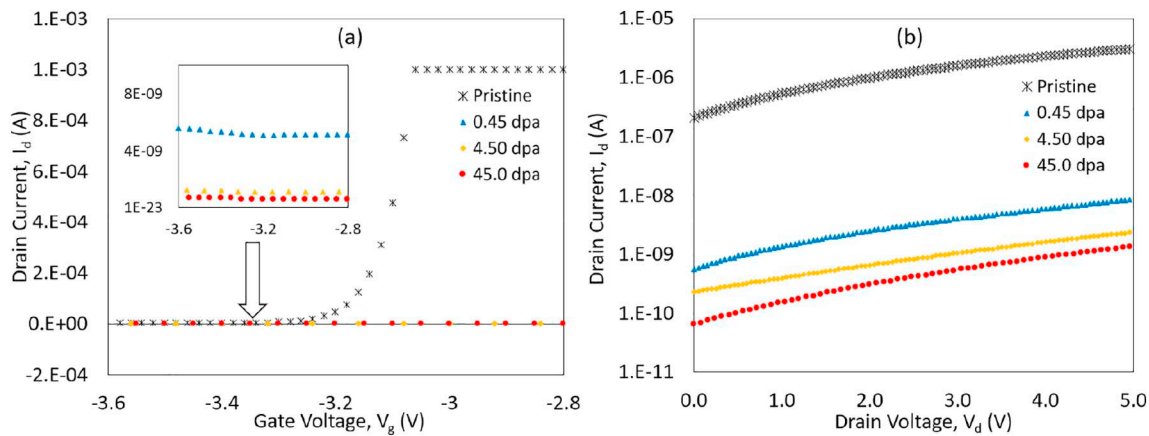


Fig. 3. (a) Transfer and (b) output characteristics curve of die-level HEMT specimens as function of ion irradiation damage in dpa.

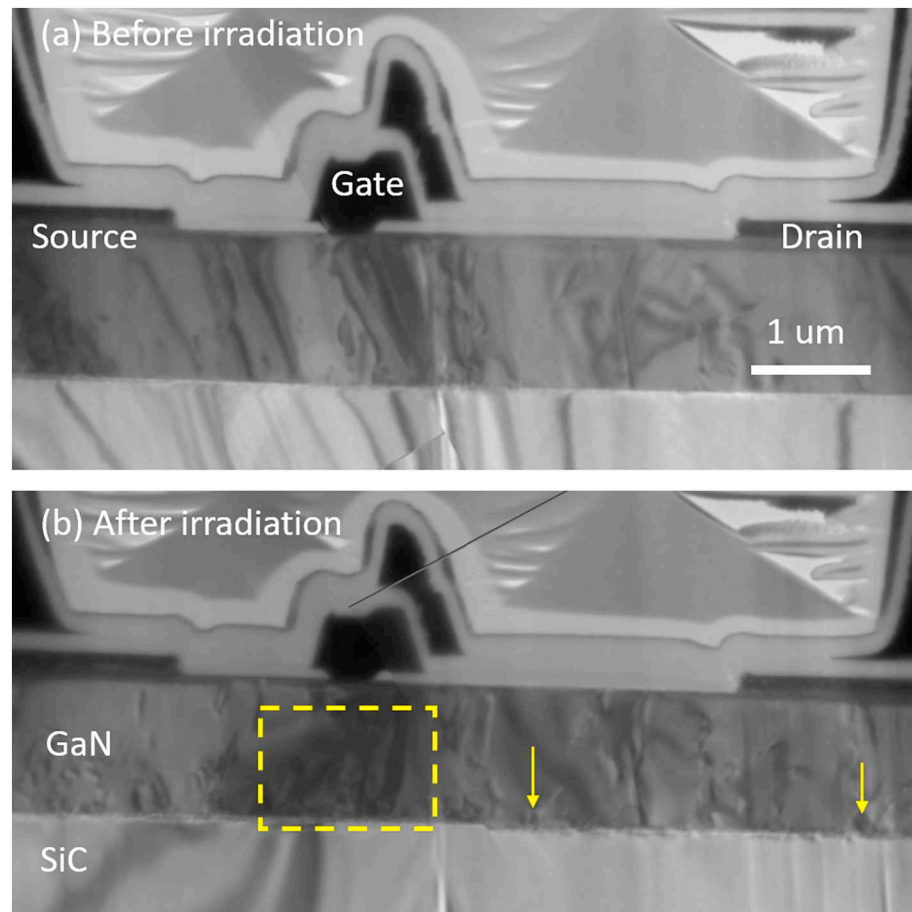


Fig. 4. Electron transparent HEMT device (a) before and (b) after 2.8 MeV Au^{4+} ion irradiation for 60 min to a fluence of at 4×10^{14} ions/cm². The dashed box shows contrast change due to point defect accumulation, while the arrows indicate dislocation activities at the GaN-SiC interface.

and bend contours could be easily distinguished by titling the sample. In our experiment, we tilt the sample by $\pm 5^\circ$ and we notice defects remain stationary whereas bend contours move. An image corresponding to this tilting has been shown as supplementary image in Fig. S1.

Fig. 6c-f capture the microstructure of the drain, gate and source at low magnification at different drain bias as indicated on Fig. 6a. In particular, three arrows are shown in Fig. 6c (labeled 2, 3 and 4) to identify location of defect clusters that appear to reproduce dislocations with stressing. With the increment of drain bias, we observe significant

change in defects in the GaN layer. For example, two dashed rectangular areas are shown in Fig. 6e to indicate the damage extended from arrows 2 and 4.

These locations make an interesting transition towards interfacial failure between the buffer and the substrate. Fig. 6f shows the image of the sample just after the failure at 10.2 V drain bias. Compared to the pristine sample, breakdown drain bias is lower, which could be attributed to defects generated at the interface of AlGaN layer as well as GaN buffer layer during the ion irradiation. In addition, pre-existing irradiation induced defects, the inverse-piezoelectric stress creates

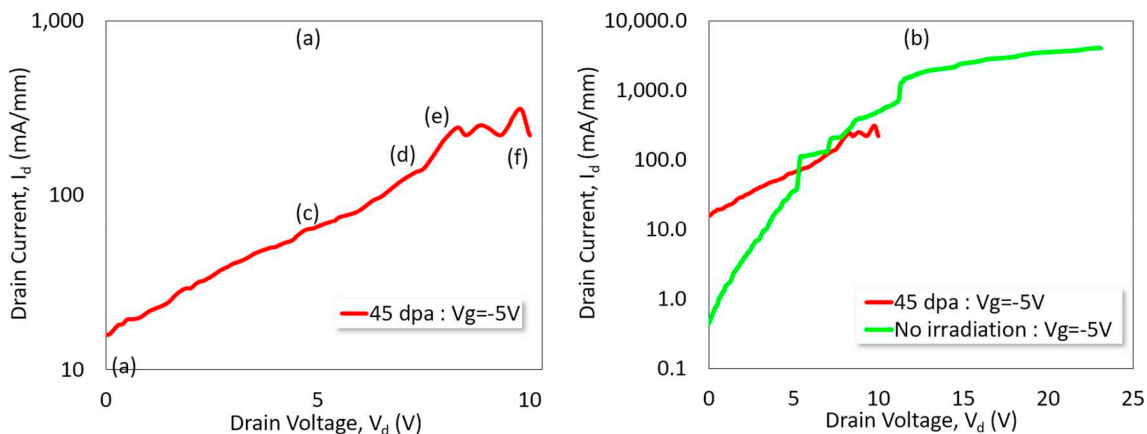


Fig. 5. (a) Drain current vs drain voltage plot of electron transparent GaN HEMT specimen in the off-state operation mode inside the TEM. The data labels correspond to the in-situ TEM images in Fig. 6. (b) Comparison between the pristine and irradiated conditions.

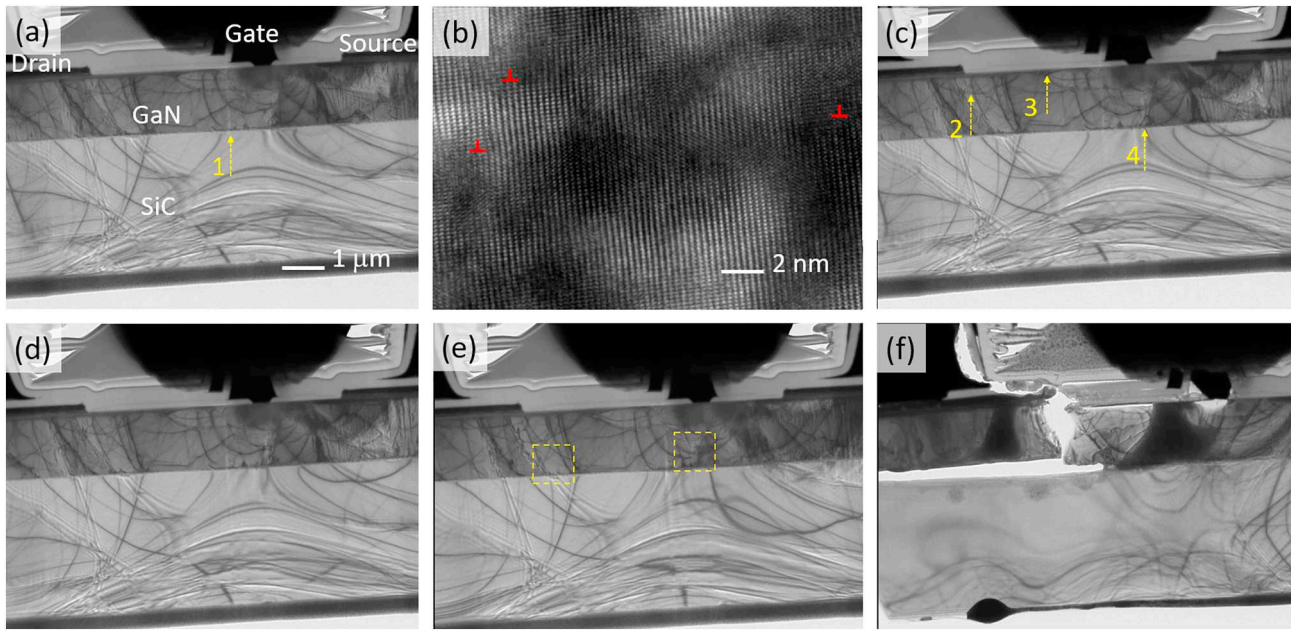


Fig. 6. Low magnification TEM images to observe source, gate and drain at the same time. Drain voltage: (a) $V_d = 0$ V, (b) TEM image of screw dislocations in buffer layer, (c) $V_d = 5$ V, (d) $V_d = 7$ V, (e) $V_d = 8.5$ V, and (f) $V_d = 10.2$ V.

dislocations during off-state loading [28,29]. These studies indicate that the resulting mechanical stresses create defects that act as traps in the GaN layer through local charge accumulations. The contribution of this study is therefore provide visual evidence of the generation of lattice (Figs. 2d and 6b) and interfacial (Fig. 3b) defects. The literature suggests that they lower the breakdown strength [30] and facilitates failure through their percolation [31].

It is well known that the drain edge of the gate electrode experiences the highest electric field during the off-state biasing [32,33]. This is consistent with our observation that ion irradiation significantly damaged the Schottky contact at the gate electrode, thus increasing the gate injection during the off-state testing. This increased gate injection could lead to the impact-ionization in the channel which in turn dictates the off-state failure as shown in Figs. 6f and 7a. A high magnification image of gate injection failure under gate electrode is shown in Fig. 7b and d. Gate injection induced high current density is sufficient to induce amorphization in the buffer layer under the gate as shown in Fig. 7b and d. During the breakdown of the buffer layer we also notice structural disintegration at the buffer-substrate interface as shown in Fig. 7c. Fig. 7d shows a zoomed view of the failed region underneath the gate. Here, the lattice appears mostly amorphized and contains agglomerations of vacancies in form of white spots; among many few of them are marked by yellow color dotted circles. Such spots are typically associated with oxygen vacancies. In this amorphous region of GaN buffer layer we also observe black spots [34] which are primarily small crystallites of GaN or diffused electrode metals as shown by cyan color dotted circle. Presence of oxygen in the HEMT could be attributed to atmospheric oxygen diffusion during sample preparation and handling during this study. The literature suggests that chemical oxidation may partially contribute to the electrical degradation [35].

Fig. 8 shows such an advantage where the experimental set-up allows us to observe high resolution imaging of defects during the in-situ TEM HEMT characterization experiments. Fig. 8a exhibits breakdown of the buffer layer and generated dislocations at the drain-gate channel. Fig. 8b and c shows bright field and high resolution TEM image of dislocations in the buffer layer respectively. These defects could act as surface traps in the buffer layer and percolation of these defects possibly lowers the breakdown voltage of the GaN HEMTs. Fig. 8d-f shows GPA technique implemented to map atomic strain in the sample

(Fig. 8c). The strain mapping process involves steps as follows: Fast Fourier Transformation (FFT) of HRTEM image, selection of two diffraction spots along lattice direction, reconstruction of image using inverse FFT (IFFT). Next, phase image, displacement field and strain field are calculated from Eqs. (1), (3), (4a), (4b) and (4c). Fig. 8d, e and f show normal strain, shear strain and corresponding lattice fringes of the sample with dislocations (as marked by white upward arrow). Fig. 8c and f show dislocations in the sample which could be distinguished by visual inspection. On the other hand, atomic strain mapping as shown in Fig. 8d and e allow us to identify individual dislocations in the sample. In our present study, we notice basal plane slip (i.e., [0001] plane) associated with $[1\bar{1}\bar{2}0]$ type dislocation. Displacement field around a dislocation is different than the pristine area of the sample which has been confirmed by atomic strain mapping. At the location of dislocations, we notice the existence of both tensile and compressive strain field as shown in Fig. 8d and e.

In-situ TEM techniques allows us to probe real-time diffusion of chemical elements during the experiments using EDS. Fig. 9 shows such an experiment to capture chemical elements diffusion at different drain bias including nitrogen (N), oxygen (O), gallium (Ga) and gold (Au). Fig. 9 indicates nitrogen deficiency under the gate electrode. It is known that nitrogen vacancies are the primary defect forms in GaN [36] under ion irradiation due to the lower displacement energy of nitrogen compared to gallium [37]. This defect could act as a trap and reduce the conductivity in GaN [38], which in turn reduces the carrier density and, increases carrier scattering at the interface of AlGaN/GaN. Thus, these ion-irradiation induced nitrogen defects could lead to accelerated breakdown compared to the pristine sample. This is shown in Fig. 9b. The nitrogen concentration in GaN layer decreases significantly near the failure zone. Fig. 9c shows the relative changes in the weight percentage of other elements in the region between the gate and the drain (the dotted rectangular box). We notice that weight percentage of both Ga and N reduces significantly after breakdown. The reduction in gallium and nitrogen could be attributed to the diffusion of GaN buffer out of rectangular box and possibly into the substrate layer. The reduction of nitrogen is more prominent than gallium. The weight percentage of gold increases after failure, which could be attributed to the diffusion from the gate electrode.

To summarize, we demonstrated a unique methodology for

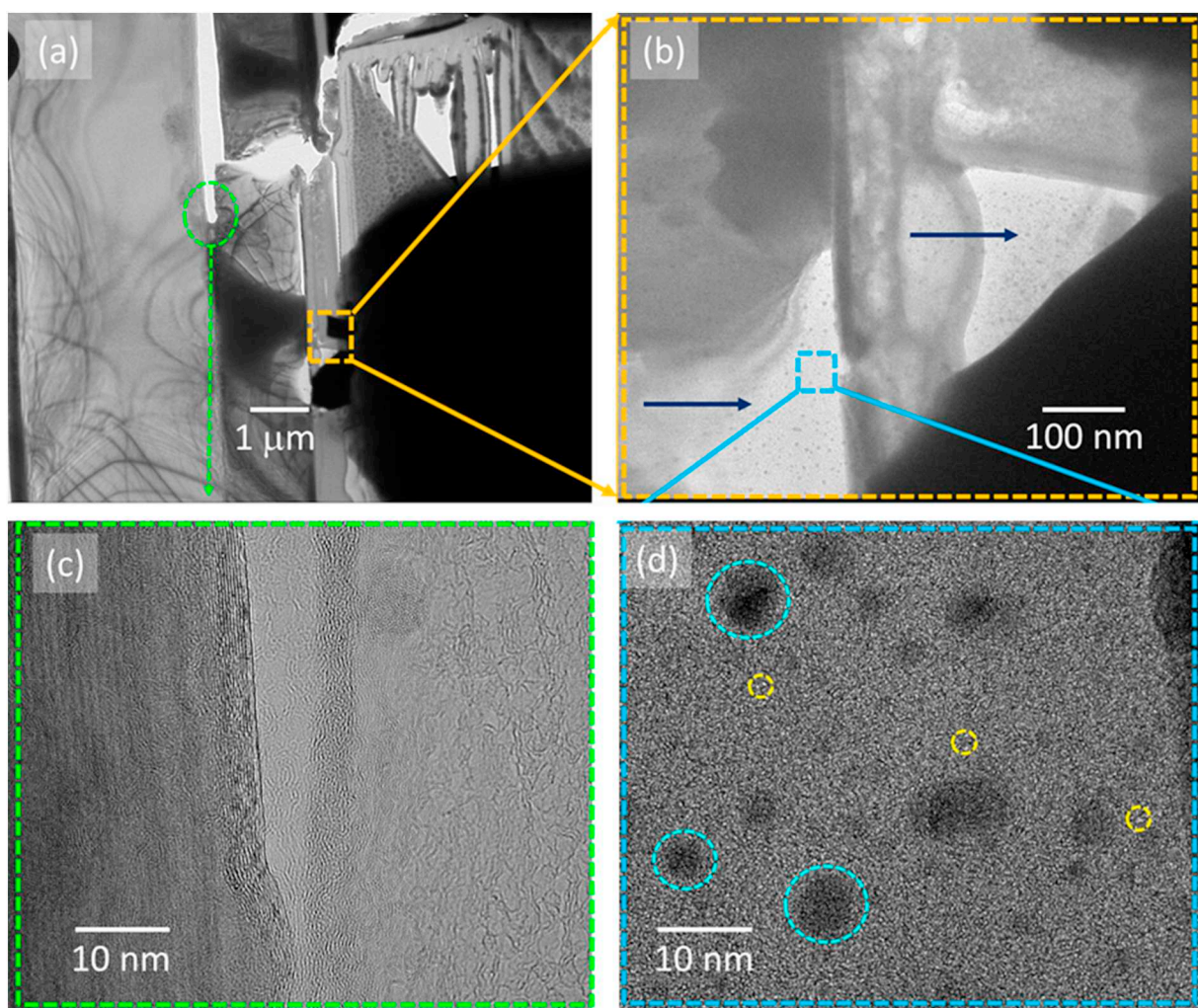


Fig. 7. (a) GaN HEMT Failure at 10.2 V drain voltage showing buffer and substrate breaching as well as gate area degradation, (b) degradation at the gate, (c) High resolution image at buffer-substrate interface, and (d) amorphization of GaN buffer layer underneath the gate.

visualizing nucleation of ion irradiation induced defects as well as their proliferation during electrical stressing of GaN-based HEMTs. Experiments were performed inside the TEM to correlate the microstructural and elemental concentration data with the electrical characteristics with the transistors. GaN HEMTs irradiated at 45 dpa showed significant number of dislocations that contributed to gate leakage that led to failure. Irradiation also increases nitrogen vacancy and metal diffusion from the gate, which are not seen in pristine HEMT failure. Future tasks include (a) scaling the physics of degradation from electron transparent device to die-level counterparts and (b) investigating the synergistic relationship between defects and diffusion leading to degradation and failure. On-state device reliability is also needed to understand the fundamentals of radiation damage in wide bandgap electronics.

4. Conclusion

Our present study investigates the effects of heavy ion irradiation on defects evolution and performance of GaN HEMTs. The following conclusions can be made from our observations:

- We observe increased defect concentrations (estimated by the number of dislocations per unit area increases in the device layer as the irradiation dose increases (measured in terms of displacement per atoms or dpa).

- Heavy ion (such as Au⁺) irradiation can generate lattice defects such as vacancies and dislocations, which could degrade device performance and accelerate permanent damage.
- Defects could act as traps which in turn degrades the carrier density and mobility in the 2DEG.
- Gate injection could lead to impact-ionization in the channel which in turn dictates the off-state failure.
- Oxide formation near the failed region of the channel layer suggests that chemical oxidation may accelerate/partially contribute to the electrical degradation.

Supplementary data to this article can be found online at <https://doi.org/10.1016/j.microrel.2019.113493>.

Declaration of competing interest

The authors declare no conflict of interest.

Acknowledgements

MAH acknowledges support from the National Science Foundation, USA through DMR grant # 1609060 and from UES Inc. NRG acknowledges support from the Air Force Office of Scientific Research grant #FA9550-19RYCOR050. This work was performed, in part, at the Center for Integrated Nanotechnologies, an Office of Science User

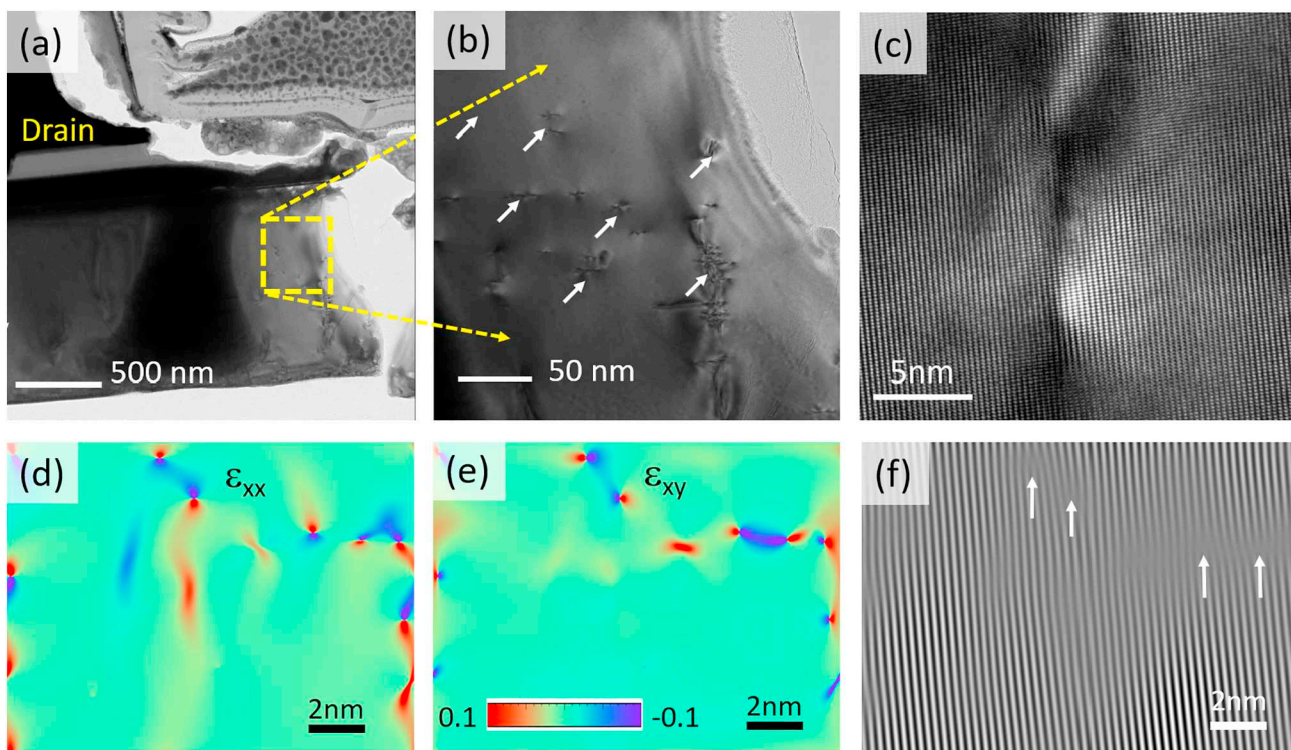


Fig. 8. (a) TEM bright field image at the drain side of drain-gate region, (b) Dislocations in the GaN layer, and (c) High resolution TEM (HRTEM) image of screw dislocations in GaN layer. (d, e) normal and shear strain field associated with dislocations and (f) Simulated lattice fringes with the dislocations.

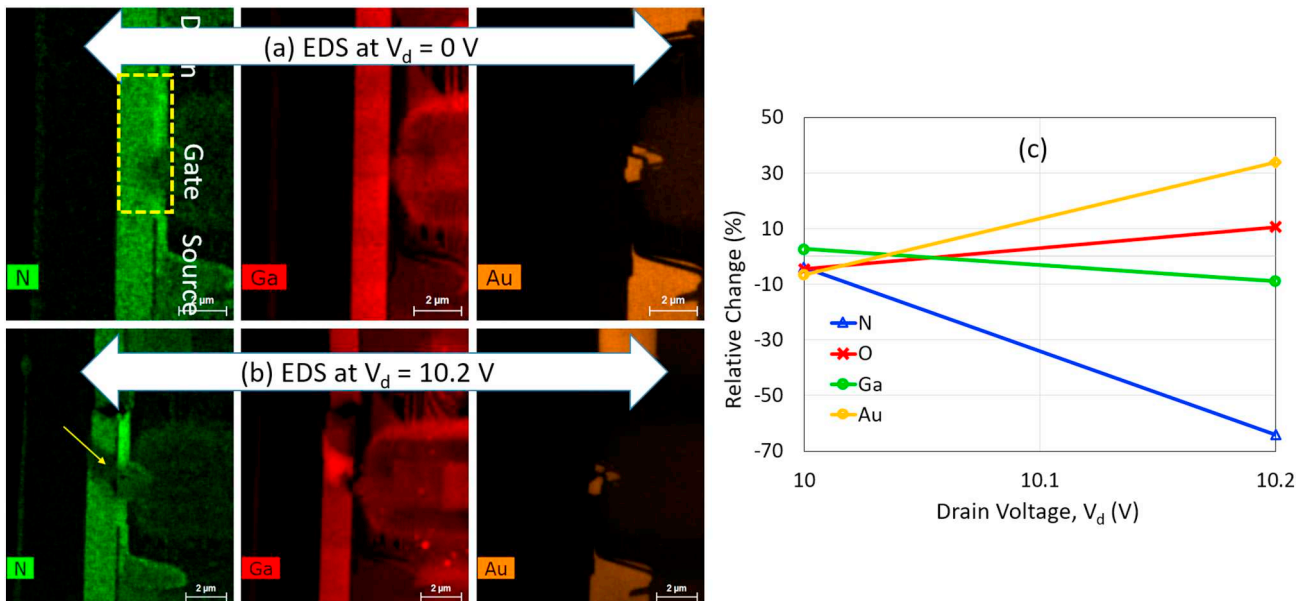


Fig. 9. EDS mapping of GaN HEMT showing diffusion of chemical elements at different drain bias: (a) $V_d = 0$ V, (b) onset of failure at $V_d = 10.2$ V, (c) Relative changes in diffusion of chemical elements obtained from EDS at these two voltages. The lines connecting the datapoints to guide the eye.

Facility operated for the U.S. Department of Energy (DOE) Office of Science. Sandia National Laboratories is a multimission laboratory managed and operated by National Technology & Engineering Solutions of Sandia, LLC, a wholly owned subsidiary of Honeywell International, Inc., for the U.S. DOE's National Nuclear Security Administration under contract DE-NA-0003525. The views expressed in the article do not necessarily represent the views of the U.S. DOE or the United States Government.

References

- [1] Y.F. Wu, et al., Very high breakdown voltage and large transconductance realized on GaN heterojunction field effect transistors, *Appl. Phys. Lett.* 69 (10) (1996) 1438–1440.
- [2] M.A. Khan, et al., GaN based heterostructure for high power devices, *Solid State Electron.* 41 (10) (1997) 1555–1559.
- [3] G. Sonia, et al., 2 MeV ion irradiation effects on AlGaN/GaN HFET devices, *Solid State Electron.* 52 (7) (2008) 1011–1017.
- [4] P. Moens, et al., Impact of buffer leakage on intrinsic reliability of 650V AlGaN/GaN HEMTs, 2015 IEEE International Electron Devices Meeting (Iedm), 2015.
- [5] D. Maier, et al., Testing the temperature limits of GaN-based HEMT devices, *IEEE*

- Trans. Device Mater. Reliab. 10 (4) (2010) 427–436.
- [6] S.M. Khanna, et al., 2 MeV proton radiation damage studies of gallium nitride films through low temperature photoluminescence spectroscopy measurements, IEEE Trans. Nucl. Sci. 47 (6) (2000) 2322–2328.
- [7] F. Gaudreau, et al., Transport properties of proton-irradiated gallium nitride-based two-dimensional electron-gas system, IEEE Trans. Nucl. Sci. 49 (6) (2002) 2702–2707.
- [8] Z.F. Lei, et al., Degradation mechanisms of AlGaN/GaN HEMTs under 800MeV bi ions irradiation, Microelectron. Reliab. 80 (2018) 312–316.
- [9] K.F. Galloway, R.D. Schrimpf, MOS device degradation due to total dose ionizing radiation in the natural space environment: a review, Microelectron. J. 21 (2) (1990) 67–81.
- [10] K. Arakawa, et al., Observation of the one-dimensional diffusion of nanometer-sized dislocation loops, Science 318 (5852) (2007) 956–959.
- [11] C. Dai, et al., Atomistic simulations of Ni segregation to irradiation induced dislocation loops in Zr-Ni alloys, Acta Mater. 140 (2017) 56–66.
- [12] S. Pearton, et al., Ionizing radiation damage effects on GaN devices, ECS Journal of solid state science and technology 5 (2) (2016) Q35–Q60.
- [13] J.C. Petrosky, et al., Trap assisted tunneling induced currents in neutron irradiated AlGaN/GaN HFETs, IEEE Trans. Nucl. Sci. 56 (5) (2009) 2905–2909.
- [14] D.C. Look, et al., Defect donor and acceptor in GaN, Phys. Rev. Lett. 79 (12) (1997) 2273–2276.
- [15] H. Xinwen, et al., The energy dependence of proton-induced degradation in AlGaN/GaN high electron mobility transistors, IEEE Trans. Nucl. Sci. 51 (2) (2004) 293–297.
- [16] A.P. Karmarkar, et al., Proton irradiation effects on GaN-based high electron-mobility transistors with Si-doped Al_xGa_{1-x}N and thick GaN cap layers, IEEE Trans. Nucl. Sci. 51 (6) (2004) 3801–3806.
- [17] B.D. White, et al., Electrical, spectral, and chemical properties of 1.8 MeV proton irradiated AlGaN/GaN HEMT structures as a function of proton fluence, IEEE Trans. Nucl. Sci. 50 (6) (2003) 1934–1941.
- [18] S.J. Cai, et al., Annealing behavior of a proton irradiated Al_xGa_{1-x}N/GaN high electron mobility transistor grown by MBE, Ieee Transactions on Electron Devices 47 (2) (2000) 304–307.
- [19] B.M. Paine, et al., Lifetesting GaN HEMTs with multiple degradation mechanisms, IEEE Trans. Device Mater. Reliab. 15 (4) (2015) 486–494.
- [20] Y. Idrees, et al., In situ study of defect accumulation in zirconium under heavy ion irradiation, J. Nucl. Mater. 433 (1–3) (2013) 95–107.
- [21] W. Baoming, et al., In-situ transmission Electron microscopy of transistor operation and failure, Nanotechnology 29 (31) (2018) 31LT01.
- [22] Z. Islam, A. Haque, N. Glavin, Real-time visualization of GaN/AlGaN high electron mobility transistor failure at off-state, Appl. Phys. Lett. 113 (18) (2018).
- [23] K. Hattar, D.C. Bufford, D.L. Buller, Concurrent in situ ion irradiation transmission electron microscope, Nucl. Instrum. Methods Phys. Res., Sect. B 338 (2014) 56–65.
- [24] J.F. Ziegler, M.D. Ziegler, J.P. Biersack, SRIM – the stopping and range of ions in matter (2010), Nucl. Instrum. Methods Phys. Res., Sect. B 268 (11–12) (2010) 1818–1823.
- [25] M.A. Haque, M.T.A. Saif, Deformation mechanisms in free-standing nanoscale thin films: a quantitative in situ transmission electron microscope study, Proc. Natl. Acad. Sci. U. S. A. 101 (17) (2004) 6335–6340.
- [26] M.J. Hytch, E. Snoeck, R. Kilaas, Quantitative measurement of displacement and strain fields from HREM micrographs, Ultramicroscopy 74 (3) (1998) 131–146.
- [27] Z. Islam, A. Haque, N. Glavin, Real-time visualization of GaN/AlGaN high electron mobility transistor failure at off-state, Appl. Phys. Lett. 113 (18) (2018) 183102.
- [28] D.A. Cullen, et al., Electroluminescence and transmission Electron microscopy characterization of reverse-biased AlGaN/GaN devices, IEEE Trans. Device Mater. Reliab. 13 (1) (2013) 126–135.
- [29] C.Y. Chang, et al., Electric-field-driven degradation in OFF-state step-stressed AlGaN/GaN high-Electron mobility transistors, IEEE Trans. Device Mater. Reliab. 11 (1) (2011) 187–193.
- [30] A.P. Zhang, et al., Microwave power SiC MESFETs and GaN HEMTs, Ieee Lester Eastman Conference on High Performance Devices, Proceedings, 2002, pp. 181–185.
- [31] P.G. Whiting, et al., Nanocrack formation in AlGaN/GaN high electron mobility transistors utilizing Ti/Al/Ni/au ohmic contacts, Microelectron. Reliab. 70 (2017) 41–48.
- [32] J.A. del Alamo, J. Joh, GaN HEMT reliability, Microelectron. Reliab. 49 (9) (2009) 1200–1206.
- [33] K.R. Bagnall, et al., Simultaneous measurement of temperature, stress, and electric field in GaN HEMTs with micro-Raman spectroscopy, Rev. Sci. Instrum. 88 (11) (2017).
- [34] W. Zhou, H.F. Greer, What can Electron microscopy tell us beyond crystal structures? Eur. J. Inorg. Chem. 2016 (7) (2016) 941–950.
- [35] G.J. Syaranamual, et al., Role of two-dimensional electron gas (2DEG) in AlGaN/GaN high electron mobility transistor (HEMT) ON-state degradation, Microelectron. Reliab. 64 (2016) 589–593.
- [36] M.G. Ganchenkova, R.M. Nieminen, Nitrogen vacancies as major point defects in gallium nitride, Phys. Rev. Lett. 96 (19) (2006).
- [37] M. Usman, et al., Electrical and structural characterization of ion implanted GaN, Nuclear Instruments & Methods in Physics Research Section B-Beam Interactions with Materials and Atoms 267 (8–9) (2009) 1561–1563.
- [38] M. Usman, A. Hallen, A. Nazir, Ion implantation induced nitrogen defects in GaN, Journal of Physics D-Applied Physics 48 (45) (2015).